

Thickness Uniformity of Spin Coated Film Influenced by Nonuniform Temperature of Substrates

Taku Ohara¹, Shinichiro Matsubara², Hirotohi Kadowaki³, Gota Kikugawa¹, Kazuhiro Takeshita⁴ and Tomoko Hamada⁴

¹Institute of Fluid Science, Tohoku University

²Mitsubishi Heavy Industries, Ltd.

³Graduate School of Engineering, Tohoku University

⁴Tokyo Electron Kyushu, Ltd.

All correspondence should be addressed to Professor Taku Ohara
Institute of Fluid Science, Tohoku University, 2-1-1 Katahira, Aoba-ku, Sendai 980-8577, Japan
E-mail: ohara@ifs.tohoku.ac.jp, Tel & Fax: +81-22-217-5277

ABSTRACT

The film thinning process in the spin coating has been analyzed by finite difference computational simulations. The coating liquid was assumed to be a solution of polymer solute and volatile organic solvent, for which Newtonian viscosity was given as a function of solute concentration. The flow of the coating liquid film that covers the entire substrate surface was analyzed where heat and mass transfer due to evaporation of solvent and heating/cooling by the substrate surface were taken into consideration. The whole process until all the solvent evaporates off the coating liquid and a dry coating film of the solute is left on the substrate was solved, and then the final film thickness was determined. Especially, influences of nonuniform substrate temperature on the profile of the final film thickness have been focused, for which three dimensional computational simulations have been performed. The case where the substrate is at rest and coating is processed only by drying the liquid film after a certain amount of solution liquid is deposited has also been analyzed and it was found that the final film thickness is larger at the local region of substrate with a higher temperature, exhibiting somewhat complicated thickness profiles.

1. INTRODUCTION

Spin coating is a technique to form a thin film on a substrate, which is utilized in various industrial processes ranging from some paint or protective coatings such as those on compact disks to some high technology coatings such as those of photoresists on LSI silicon wafers. In the spin coating processes, a coating liquid that contains a coating material as a solute in a solvent is deposited on a substrate. The amount of the coating liquid deposited on the substrate is typically of the order of 10^{-6} m³ to coat the substrates with areas of the order of 10^{-2} – 10^{-1} m². The amount of the deposited coating liquid is on a general decreasing trend to reduce the wasted liquids. The deposited liquid spreads on the substrate driven by the centrifugal force due to the rotation of substrates at typically several thousand rpm, and covers all over the substrate in a short time. In the following period of process, most of the deposited coating liquid is swept off the substrate until the process stops, and the amount of the residual liquid on the substrate determines the thickness of the final coating film.

The concept of two stage model is often applied to model the process of spin coating. The first stage is the process in which the coating liquid spreads on the substrate, and this stage ends when the coating liquid covers all over the substrate. In this stage, the front of the spreading liquids exhibits complicated dynamic behavior governed by the interfacial phenomena at the solid-liquid-air contact line, as was discussed by Alekseev et al.[1] and Schwartz and Roy [2]. In the following stage where the coating liquid covers the entire substrate surface, the interfacial phenomena have less influence on the flow and fluid dynamics of the film flow governs the film thinning process. The present study treats the heat and mass transfer of the film flow in this second stage.

The most basic view of the film flow on a rotating substrate has been brought by Emslie et al.[3]. Their simple 1-D governing equation was derived for the fully developed radial flow of Newtonian

liquids as a balance between centrifugal force and viscous force due to gradient of radial flow velocity. The developing flow of Newtonian liquids on a suddenly started rotating disk has been analyzed by Higgins et al. [4, 5] and Sukanek [6]. Through these studies, it has been shown that Newtonian liquids form a film flow of uniform thickness on a rotating disk. Although most of the coating liquids are solution of polymer materials which exhibits non-Newtonian viscosity, they come close to Newtonian when the shear rate is small, which is attained in the case of thin film thickness. Thus, the above results hold importance for such polymer solutions. Flow of non-Newtonian liquids have been analyzed by Acrivos et al. [7] for power-law liquids, Jenekhe and Schuldt for Carreau liquids [8] and Bingham liquids [9], Sukanek [10] for the truncated power-law liquids, Britten and Thomas [11] for Carreau liquids, Burgess and Wilson [12] for Bingham liquids. Through these studies, it has been shown that the power-law and Bingham liquids does not result in uniform thickness.

The purely hydrodynamics studies mentioned above give transient liquid film thickness that decreases with time to infinitely small value, while in most of the practical applications, the flow stops automatically at a certain process time and the film thickness at this final state is reproduced with a satisfactory accuracy. This is the case in which coating liquids are solutions with volatile solvents. The solvent evaporates during the process promoted by the flow of ambient air, which is driven by the rotation of the disk. The solute concentration in the liquid film increases, which results in increase in liquid viscosity, and finally the flow stops leaving a dry film of the solute on the disk. To analyze this process and predict the final film thickness, heat and mass transfer in the film with the solvent evaporation at the surface of the liquid film should be solved to determine the transient temperature and solute concentration taking the change in viscosity into account. Meyerhofer [13], Jenekhe [14] and Sukanek [15] have done that using film-averaged equations. Bornside et al. [16,17], Lawrence [18,19], and Yonkoski and Soane [20] have also proposed models that give the final film thickness. One of the present authors [21] have formulated a set of 1-dimensional (1-D) governing equations of heat, mass and momentum conservation for the coating liquid and the ambient air, which reproduced the final film thickness obtained in the experiment of Flack et al. [22]

Although it is a well-established fact that spin coating on an infinite substrate in an infinite calm atmosphere is reduced to a 1-D phenomenon with similar solutions that leads to uniform final film thickness, some deviation from the above 1-D conditions makes nonuniform distribution of final film thickness in practical applications. Flow of the ambient air, transition to turbulence at the outer area of the rotating substrate, casing of the spin coater that disturbs the flow of the ambient air, nonuniform temperature distribution of the substrate and ambient air, and finite diameter of the substrate may break the 1-D characteristics. The present study aims to analyze such phenomena by using 3-D computational simulations. Especially influence of nonuniform distribution of substrate temperature has been focused on. This often occurs in practical coating processes, which may be caused by various factors such as the chuck on the reverse side, nonuniform thickness of the substrate disk, and adhesion of some particles. Birnie [23,24] has observed an increase of final film thickness at the position of the chuck, which was attributed to the increased thermal capacity that works against cooling due to solvent evaporation. In the present study, 3-D computational simulations for a liquid film on a planar rotating substrate having a hot or cold local area have been performed. Heat and fluid flow on the substrate and film thickness profiles on the hot or cold local area are discussed.

The process in which a solvent evaporates leaving a thin film of a solute on a substrate at rest, which can be considered as a special case of spin coating with the spinning speed of zero, is being utilized in some industrial applications in these days. In this case, the amount of solute final film thickness is determined simply by the initial amount of solution on the substrate with a given concentration, because no solution is swept off the substrate. The problem that comes out in this application is a nonuniformity of resulted final film thickness caused by a nonuniform temperature of the substrate. This case is also discussed in the present study.

2. COMPUTATIONAL SIMULATION

A liquid film flow covering a substrate rotating at a constant speed is solved by the finite difference method. The liquid is a solution with a volatile solvent, for which viscosity is given as a function of solute concentration. The solvent evaporates from the free surface of the liquid film, causing an increase in the solute concentration at the surface, which leads to a concentration increase all over the film thickness due to mass diffusion. The thickness of the liquid film decreases due both to radial flow driven by the centrifugal forces and to the solvent evaporation. The substrate has a temperature

distribution and heat transfer occurs in the liquid film. The process of the radial flow and the solvent evaporation ceases when all the solvent has evaporated and a film of the solute is left on the substrate.

Evaporation of solvent and relevant mass transfer in the liquid film, heat transfer, and change in liquid viscosity as a function of concentration should be considered to model the above phenomena. Our simulation model applied here is a straightforward extension of the 1-D model utilized by one of the authors. [21] The 3-D governing equations are given in cylindrical coordinates as follows.

The equation of continuity

$$\frac{\partial \rho}{\partial t} + \frac{1}{r} \frac{\partial}{\partial r} (r \rho v_r) + \frac{1}{r} \frac{\partial}{\partial \theta} (\rho v_\theta) + \frac{\partial}{\partial z} (\rho v_z) = 0, \quad (1)$$

where t , r , θ and z denote time, radial coordinates, azimuthal coordinates, and axial coordinates, respectively. v_r , v_θ and v_z are flow velocities. ρ is density.

The equation of momentum conservation

$$\begin{aligned} & \frac{\partial \rho v_r}{\partial t} + \frac{1}{r} \frac{\partial}{\partial r} (r \rho v_r^2) + \frac{1}{r} \frac{\partial}{\partial \theta} (\rho v_r v_\theta) + \frac{\partial}{\partial z} (\rho v_r v_z) - \rho \frac{v_\theta^2}{r} \\ & = -\frac{\partial p}{\partial r} + \left(\frac{1}{r} \frac{\partial}{\partial r} (r \tau_{rr}) + \frac{1}{r} \frac{\partial \tau_{r\theta}}{\partial \theta} - \frac{\tau_{\theta\theta}}{r} + \frac{\partial \tau_{rz}}{\partial z} \right), \end{aligned} \quad (2)$$

$$\begin{aligned} & \frac{\partial \rho v_\theta}{\partial t} + \frac{1}{r} \frac{\partial}{\partial r} (r \rho v_r v_\theta) + \frac{1}{r} \frac{\partial}{\partial \theta} (\rho v_\theta^2) + \frac{\partial}{\partial z} (\rho v_\theta v_z) + \rho \frac{v_r v_\theta}{r} \\ & = -\frac{1}{r} \frac{\partial p}{\partial \theta} + \left(\frac{1}{r^2} \frac{\partial}{\partial r} (r^2 \tau_{r\theta}) + \frac{1}{r} \frac{\partial \tau_{\theta\theta}}{\partial \theta} + \frac{\partial \tau_{\theta z}}{\partial z} \right), \end{aligned} \quad (3)$$

$$\begin{aligned} & \frac{\partial \rho v_z}{\partial t} + \frac{1}{r} \frac{\partial}{\partial r} (r \rho v_r v_z) + \frac{1}{r} \frac{\partial}{\partial \theta} (\rho v_\theta v_z) + \frac{\partial}{\partial z} (\rho v_z^2) \\ & = -\frac{\partial p}{\partial z} + \left(\frac{1}{r} \frac{\partial}{\partial r} (r \tau_{rz}) + \frac{1}{r} \frac{\partial \tau_{\theta z}}{\partial \theta} + \frac{\partial \tau_{zz}}{\partial z} \right) + \rho g_z, \end{aligned} \quad (4)$$

where p and g_z denote pressure and the acceleration of gravity, respectively. The viscous shear stress, τ , is defined as follows based on the assumption that the liquid is Newtonian.

$$\tau_{rr} = \mu \left[2 \frac{\partial v_r}{\partial r} - \frac{2}{3} (\nabla \cdot \mathbf{v}) \right],$$

$$\tau_{\theta\theta} = \mu \left[2 \left(\frac{1}{r} \frac{\partial v_\theta}{\partial \theta} + \frac{v_r}{r} \right) - \frac{2}{3} (\nabla \cdot \mathbf{v}) \right],$$

$$\tau_{zz} = \mu \left[2 \frac{\partial v_z}{\partial z} - \frac{2}{3} (\nabla \cdot \mathbf{v}) \right],$$

$$\tau_{r\theta} = \mu \left[r \frac{\partial}{\partial r} \left(\frac{v_\theta}{r} \right) + \frac{1}{r} \frac{\partial v_r}{\partial \theta} \right],$$

$$\tau_{\theta z} = \mu \left[\frac{\partial v_\theta}{\partial r} + \frac{1}{r} \frac{\partial v_z}{\partial \theta} \right],$$

$$\tau_{rz} = \mu \left[\frac{\partial v_z}{\partial r} + \frac{\partial v_r}{\partial z} \right],$$

where μ is the viscosity. $(\nabla \cdot \mathbf{v})$ is defined by

$$(\nabla \cdot \mathbf{v}) = \frac{1}{r} \frac{\partial}{\partial r} (rv_r) + \frac{1}{r} \frac{\partial v_\theta}{\partial \theta} + \frac{\partial v_z}{\partial z}.$$

The equation of thermal energy conservation

$$\begin{aligned} \frac{\partial \rho h}{\partial t} + \frac{1}{r} \frac{\partial}{\partial r} (rv_r \rho h) + \frac{1}{r} \frac{\partial}{\partial \theta} (v_\theta \rho h) + \frac{\partial}{\partial z} (v_z \rho h) \\ = \frac{1}{r} \frac{\partial}{\partial r} \left(r \lambda \frac{\partial T}{\partial r} \right) + \frac{1}{r^2} \frac{\partial}{\partial \theta} \left(\lambda \frac{\partial T}{\partial \theta} \right) + \frac{\partial}{\partial z} \left(\lambda \frac{\partial T}{\partial z} \right), \end{aligned} \quad (5)$$

where h , T and λ denote enthalpy, temperature and thermal conductivity, respectively. Here, the work by viscous and pressure forces are neglected.

The conservation equation of mass of solute

$$\begin{aligned} \frac{\partial \rho_1}{\partial t} + \frac{1}{r} \frac{\partial}{\partial r} (rv_r \rho_1) + \frac{1}{r} \frac{\partial}{\partial \theta} (v_\theta \rho_1) + \frac{\partial}{\partial z} (v_z \rho_1) \\ = \frac{1}{r} \frac{\partial}{\partial r} \left(r \rho D \frac{\partial C}{\partial r} \right) + \frac{1}{r^2} \frac{\partial}{\partial \theta} \left(\rho D \frac{\partial C}{\partial \theta} \right) + \frac{\partial}{\partial z} \left(\rho D \frac{\partial C}{\partial z} \right), \end{aligned} \quad (6)$$

where ρ_1 and D denote density of the solute and mass diffusion coefficient, respectively. C is the mass concentration of the solute defined as $C = \rho_1 / \rho$.

In the present study, a liquid flow that covers a substrate is examined on the assumption that the liquid is filmwise and nearly flat with an almost uniform thickness. The transient film thickness, $H = H(r, \theta, t)$, was determined by the following equation.

$$\frac{\partial H}{\partial t} + v_{r,s} \frac{\partial H}{\partial r} + v_{\theta,s} \frac{\partial H}{\partial \theta} = v_{s,z}, \quad (7)$$

where $v_{r,s}$ and $v_{\theta,s}$ are v_r and v_θ at the surface of the liquid film, respectively. $v_{s,z}$ denote axial velocity of liquid surface determined by both the flow velocity, $v_{z,s}$, and evaporation of solvent, which will be discussed later.

The following boundary conditions were applied to the above governing equations. At the surface of the disk, flow velocity and liquid temperature are equal to those of the rotating substrate. i.e.,

$$v_r = 0, \quad v_\theta = r\omega, \quad v_z = 0, \quad T = T_w, \quad (8a)$$

where ω is the angular velocity of the substrate. Temperature of the substrate is assumed to be constant at T_w . The condition of no mass flux at the surface of the substrate gives

$$\frac{\partial C}{\partial z} = 0. \quad (8b)$$

At the free surface of the liquid, it is assumed that the z axis is normal to the surface. As the shear stress at the surface given by the flow of ambient atmosphere is negligible, the following zero-shear condition was applied.

$$\frac{\partial v_r}{\partial z} = 0, \quad \frac{\partial v_\theta}{\partial z} = 0. \quad (9a)$$

Here, the surface shear due to the gradient of surface tension caused by a nonuniform temperature or concentration, i.e., the Marangoni effect, was neglected as it is minor in the present case where the liquid flow is driven by the dominating force balance between strong centrifugal force and shear viscosity.

The axial velocity of moving liquid surface, $v_{s,z}$, which appeared in eqn (7), is given by the following equation considering the liquid flow and the evaporation of solvent.

$$v_{s,z} = v_{z,s} - \frac{\dot{m}}{\rho}, \quad (9b)$$

where \dot{m} denotes evaporation rate of the solvent, which will be described later. The boundary condition for the temperature at the free surface is given by a heat balance among heat conduction in the liquid, evaporative cooling, and heat transfer from the ambient air as follows.

$$-\lambda \left(\frac{\partial T}{\partial z} \right)_s + \alpha(T_s - T_g) = \dot{m}L, \quad (9c)$$

where T_s and T_g denote temperatures at the liquid surface and the ambient atmosphere, respectively. L is the latent heat for evaporation of the solvent. α is the heat transfer coefficient for a rotating disk and ambient air flow, which is approximated by an empirical formula [25],

$$\alpha = 0.38\lambda_g \sqrt{\frac{\omega}{\nu_g}},$$

where λ_g and ν_g denote thermal conductivity and kinetic viscosity of ambient air, respectively. Here the heat transfer coefficient is given as being uniform over the liquid surface, which is appropriate because of the one-dimensional nature of the spinning system as is described later in 3.1. This assumption was applied even in the cases of nonuniform substrate temperature, as the deviation from the one-dimensional similarity solution is small and the influence of the deviation on the heat transfer coefficient is considered to be negligible.

Evaporation of solvent at the liquid surface results in an increase in the solute concentration at the surface, which gives the following boundary condition for the solute transport equation.[21]

$$\left(\frac{\partial C}{\partial z} \right)_s = \frac{\dot{m}C}{D\rho}. \quad (9d)$$

The pressure of the liquid at its free surface is given by the surface tension according to the curvature of the surface. i.e.,

$$p_s = 2\sigma\kappa, \quad (9e)$$

where σ and κ denote properties of surface tension of the liquid and curvature of the free surface given by the following equation.

$$\kappa = \frac{S_1 \cdot S_c + S_3 \cdot S_a - 2S_2 \cdot S_b}{2(S_1 \cdot S_3 - S_2^2)},$$

$$S_1 = 1 + \left(\frac{\partial H}{\partial r} \right)^2,$$

$$S_2 = \frac{\partial H}{\partial r} \cdot \frac{\partial H}{\partial \theta},$$

$$S_3 = r^2 + \left(\frac{\partial H}{\partial \theta} \right)^2,$$

$$S_a = \frac{r \frac{\partial^2 H}{\partial r^2}}{\sqrt{r^2 + r^2 \left(\frac{\partial^2 H}{\partial r^2} \right)^2 + \left(\frac{\partial^2 H}{\partial \theta^2} \right)^2}},$$

$$S_b = \frac{r \frac{\partial^2 H}{\partial r \partial \theta}}{\sqrt{r^2 + r^2 \left(\frac{\partial^2 H}{\partial r^2} \right)^2 + \left(\frac{\partial^2 H}{\partial \theta^2} \right)^2}},$$

$$S_c = \frac{r \frac{\partial^2 H}{\partial \theta^2}}{\sqrt{r^2 + r^2 \left(\frac{\partial^2 H}{\partial r^2} \right)^2 + \left(\frac{\partial^2 H}{\partial \theta^2} \right)^2}}.$$

In the present study, the liquid flow is assumed to be very shallow and slow, and the hydrostatic approximation was applied to determine the pressure in the liquid. i.e.,

$$p(r, \theta, z, t) = p_s(r, \theta, t) + \rho g_z (H(r, \theta, t) - z). \quad (10)$$

In the simulations, the conservation equations for the momentum in the radial and azimuthal directions, eqns (2) and (3), were solved using the above pressure, and the axial flow velocity was determined to satisfy the mass conservation expressed by eqn (1). Thus, the conservation equation for the momentum in the axial direction, eqn (4), was not utilized.

The finite difference method was applied to solve the above set of equations. The calculation domain is $0 \leq r \leq 80$ mm and $0 \leq \theta \leq 2\pi$. Dimension of the calculation domain in the z direction is maintained so that it is larger than the maximum thickness of the liquid film at any time; the dimension is reduced to its half value when the thickness of the liquid film is reduced below the half value of the dimension. The domain was divided into $200 \times 120 \times 20$ calculation cells in the r , θ and z directions, respectively, with the cell sizes of $\Delta r = 0.4$ mm and $\Delta \theta = \pi/60$ rad. The cell size in the z direction, Δz , is reduced along with the reduction of the dimension of the calculation domain in the manner mentioned above. The difference equations to be solved were obtained using the 2nd-order central difference method for spatial derivatives except for the convective terms in the conservation equations of thermal energy and solute mass, for which a hybrid scheme with the 2nd-order central difference in cases of the cell Peclet number $Pe \leq 2$ and the 1st-order upwind difference otherwise. For the time integration, 1st-order Euler explicit method was applied for the transport in the directions of r and θ . For the z direction, Euler implicit method was applied, which was solved by the TDMA scheme.

A solution of polymethyl methacrylate (PMMA) with chlorobenzene solvent was assumed for the coating liquid, and thermophysical properties approximated for the solution were applied. Viscosity was assumed as a function of solute concentration as

$$\mu = 2.62 \times 10^5 C^{2.33} \exp\left(\frac{C-1}{0.083-0.04C}\right) \text{ Pa}\cdot\text{s}, \quad (11a)$$

where dependency on temperature was ignored based on an assumption that temperature change exhibited in the present study is small. Figure 1 shows the viscosity as a function of solute concentration.

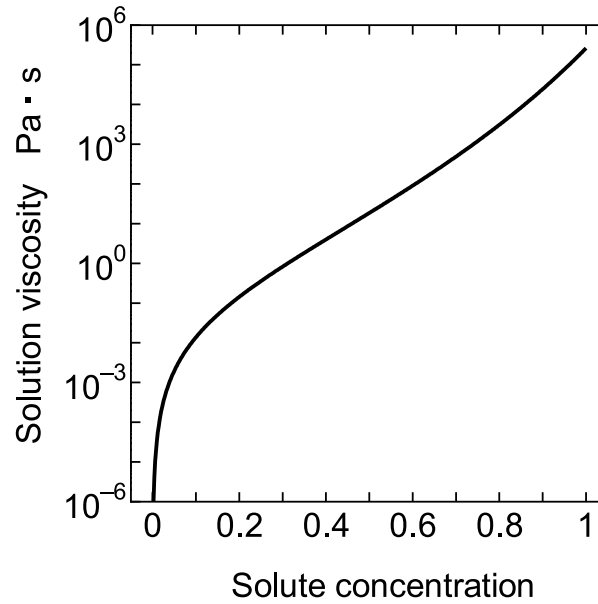


Figure 1. Viscosity of the solution as a function of the solute concentration.

Density, thermal conductivity, diffusion coefficient and surface tension, ρ , λ , D and σ , respectively, were assumed to be constant as

$$\rho = 1.14 \times 10^3 \text{ kg/m}^3, \quad (11b)$$

$$\lambda = 0.150 \text{ W/(m} \cdot \text{K)}, \quad (11c)$$

$$D = 5.80 \times 10^{-10} \text{ m}^2/\text{s}, \quad (11d)$$

$$\sigma = 0.020 \text{ N/m}. \quad (11e)$$

Enthalpy of the solution and latent heat of vaporization for solvent were assumed to be linearly dependent on temperature in the narrow range of temperature change assumed in the present study as

$$h = 1.37 \times 10^3 T \text{ J/kg}, \quad (11f)$$

$$L = 4.127 \times 10^4 (632.4 - T_s) \text{ J/kg}, \quad (11g)$$

where T_s denote temperature of the liquid at the surface.

Evaporation rate of the solvent, \dot{m} , defined as mass of evaporating solvent per unit area and time, was approximated as a function of temperature and rotation speed of the substrate by the following equation.

$$\dot{m} = 5.83 \times 10^{-8} \omega^{0.5} \alpha \exp \left[20.9604 - \frac{3296.12}{T_s - 55.60} \right] \quad (11h)$$

$$\alpha = \exp[\ln(1 - C_s) + C_s + 0.44C_s^2].$$

Here, C_s represents concentration of solute at the surface. This equation reproduces the evaporation rate predicted by a more complete simulation [21] with its dependencies on temperature and solute concentration sufficiently for the present purpose, although it is a somewhat rough representation. Figure 2 shows dependency of the evaporation rate on the solute concentration at several temperatures. Increase of temperature by 5 K results in increase of evaporation rate by approximately 30 %.

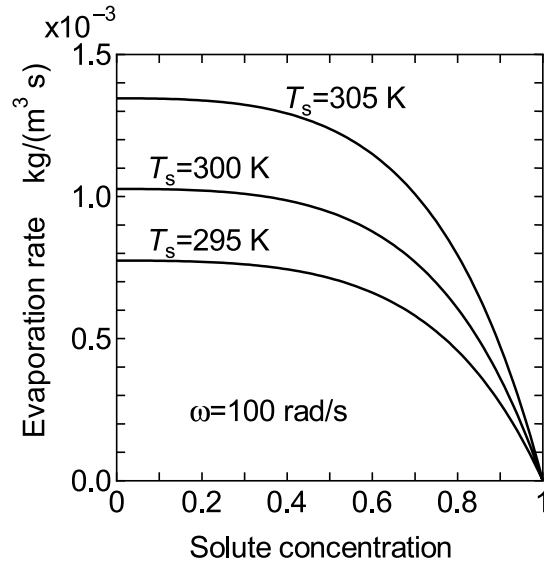


Figure 2. Rate of solvent evaporation as a function of the solute concentration at the surface of the solution liquid film. $\omega=100$ rad/s.

In all the cases simulated in this study, the liquid film was assumed to be at rest with a uniform thickness and temperature on the substrate initially, and start to flow in its thinning process after an impulsive start of the substrate. The initial condition applied was as follows.

$$\begin{aligned}
 v_r &= 0, \\
 v_\theta &= 0, \\
 v_z &= 0, \\
 C &= C_0, \\
 T &= T_0, \\
 H &= H_0,
 \end{aligned} \tag{12}$$

where C_0 , T_0 and H_0 denote initial solute concentration, temperature, and thickness, which were assumed to be uniform over the liquid film.

3. RESULTS AND DISCUSSIONS

3.1 Case of Uniform Substrate Temperature

Before the simulation of nonuniform substrate temperature cases, some cases with uniform substrate temperatures were simulated. In this case, the following similarity solutions exist for velocity, film thickness, temperature and solute concentration [21]:

$$\begin{aligned}
 v_r(r, \theta, z, t) &= rV_r(z, t), \\
 v_\theta(r, \theta, z, t) &= rV_\theta(z, t), \\
 v_z(r, \theta, z, t) &= V_z(z, t), \\
 H(r, \theta, t) &= H(t), \\
 C(r, \theta, z, t) &= C(z, t), \\
 T(r, \theta, z, t) &= T(z, t).
 \end{aligned} \tag{13}$$

Thus, the field is one-dimensional in nature. These 1-D similarity solutions have also been reproduced in the present 3-D simulation with uniform substrate temperature, and some results are displayed here to describe the basic phenomena in the film flow of spin coating. Here, the initial film thickness $H_0=1\text{mm}$, temperatures are $T_0=T_w=T_g=300\text{ K}$, initial solute concentration $C_0=0.06$, and the spinning speed $\omega=100\text{ rad/s}$.

Figure 3 shows the transient film thickness, which is averaged over the film as follows.

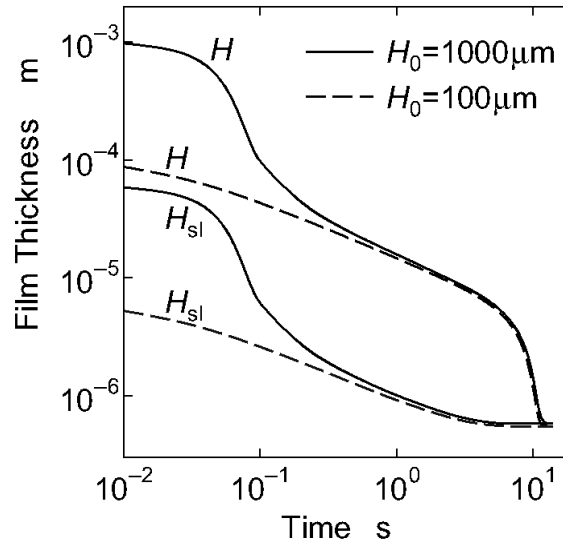


Figure 3. Transient average thickness of the liquid film, H , and solute portion of the film thickness, H_{sl} , defined by eqns (14) and (15). $H_0=1\text{ mm}$ or $100\text{ }\mu\text{m}$, $T_0=T_w=T_g=300\text{ K}$, $C_0=0.06$, and $\omega=100\text{ rad/s}$.

$$H = \frac{1}{\pi R^2} \int_0^{2\pi} \int_0^R H(r, \theta) r dr d\theta, \quad (14)$$

where R denotes the radius of the calculation domain. In the figure, the solute portion of the solution thickness, H_{sl} , is also plotted, which indicate the mass of solute on the substrate given by

$$H_{sl} = \frac{1}{\pi R^2} \int_0^{2\pi} \int_0^R \int_0^H C r dz dr d\theta. \quad (15)$$

The solution thickness, H , decreases due both to the radial flow driven by the centrifugal forces during spinning and to the evaporation of solvent, as expressed by eqn (9b). On the other hand, the mass of solution on the substrate, represented by H_{sl} , which determines the film thickness when the spinning is stopped at the time and the solvent is removed by air drying or baking, decreases due only to the radial flow. Figure 4 shows these two factors, where each of the two terms of the right side of eqn (9b) is plotted. After the time range of $t < 10^{-1}\text{ s}$ during which the solution liquid is accelerated by the suddenly started rotating substrate, the liquid film thickness decreases monotonously; this is mainly due to the radial flow driven by the spinning. In this stage, the liquid film thickness, H , and its solute portion, H_{sl} , show a quite similar time response in Fig. 3. As the thickness decreases, the film thinning rate due to the radial flow is reduced, while the evaporation of solvent keeps its magnitude. Approximately at $t = 3\text{ s}$, the dominant factor in the film thinning is switched from the radial flow of the liquid to the solvent evaporation. After this, the mass of solute on the substrate indicated by H_{sl} no longer decreases, while the liquid film thickness, H , continues to decrease. Thus, H approaches H_{sl} . In the final stage, increase in the solute concentration in the liquid film reduces the rate of solvent evaporation and finally, H reaches H_{sl} when we have a dry film of the solute on the substrate.

Thickness Uniformity of Spin Coated Film Influenced by Nonuniform Temperature of Substrates

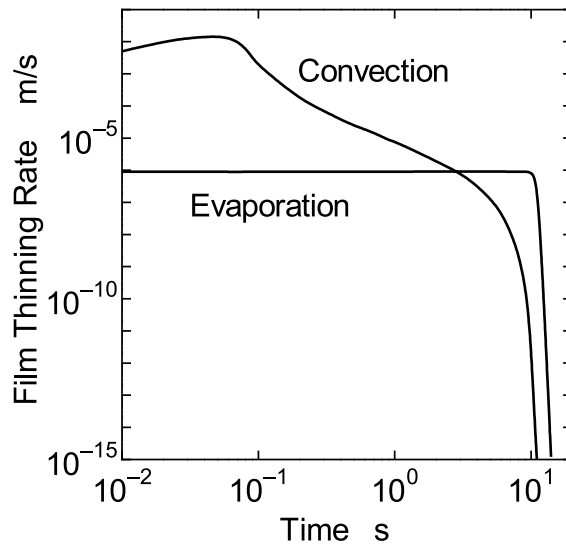


Figure 4. Film thinning rates due to the radial convective flow and the solvent evaporation defined by eqn (9b) for the same conditions as Fig. 3. $H_0=1$ mm.

The transient response of the film thickness and its final value agree with the results of the authors' 1-D simulation and experiment. [21,26] It was observed that the final film thickness is proportional to $\omega^{-0.5}$, and remains nearly unaffected by the initial film thickness, both of which have been reported by many studies.

The process is influenced by the substrate temperature. The response of the final film thickness to the uniform substrate temperature observed by the present simulations for the cases of $T_0=T_g=300$ K, $H_0=100$ μ m, $C_0=0.06$, and $\omega=100$ rad/s is shown in Fig. 5. Higher substrate temperature causes higher rate of solvent evaporation, which leads to shorter spinning time for the film to be dried, and thicker final film is obtained.

The results described in this section are for the case of uniform substrate temperature. On the other hand, in case where temperature of only a part of the substrate is elevated, local increase of solvent evaporation produces more complex 3-D phenomena, which is described in the next section.

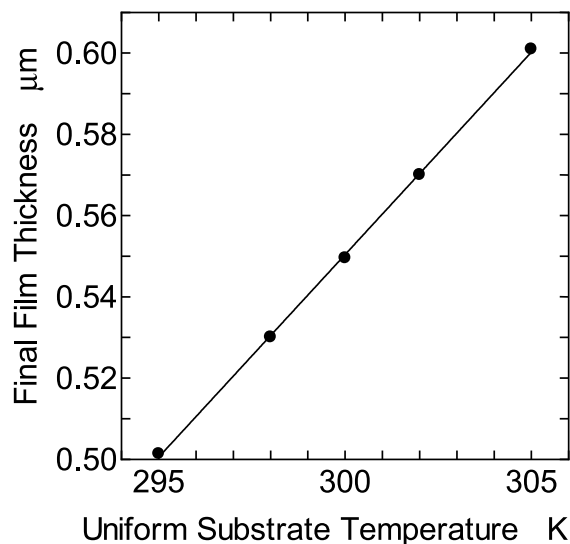


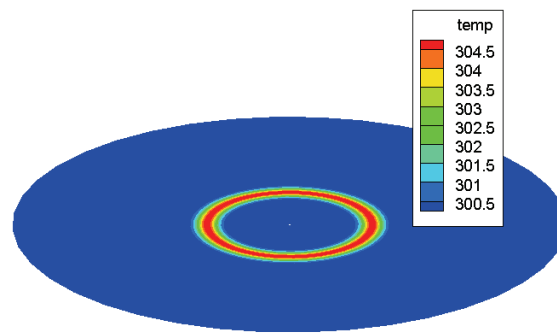
Figure 5. Response of final film thickness to the uniform substrate temperature, T_w , where $T_0=T_g=300$ K, $H_0=100$ μ m, $C_0=0.06$, and $\omega=100$ rad/s. The straight line fitted to the data (dots) is only for clarity.

3.2 Case of Nonuniform Substrate Temperature

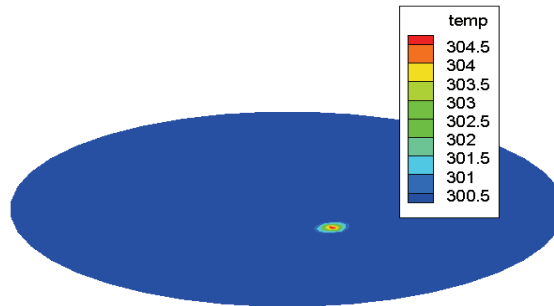
The cases where a portion of the substrate is kept at higher or lower temperature than the other region of the substrate are discussed in this section. A ring-like or spot-like high or low temperature region is placed on the substrate as shown in Fig. 6. For the “hot ring” case, the substrate temperature, T_w , is given as a function of r by

$$T_w = T_b + \Delta T \exp[k(r - r_0)^2], \quad (16)$$

where T_b and ΔT denote the base temperature and the temperature rise at the peak of temperature in the hot ring. k is a constant to determine the width of the hot ring, which was fixed to be $-1.0 \times 10^5 \text{ m}^{-2}$ in the present simulations. r_0 is the radial location of the center of the hot arc, which was fixed to be 0.024 m in the present simulations. T_b was fixed to be 300 K and several values were given for ΔT in the range $-5 < \Delta T < 5$ K. The distribution of substrate temperature for the case of $\Delta T=5$ K is shown in Fig. 7.



(a) Hot ring



(b) Hot spot

Figure 6. “Hot ring” and “hot spot” on the substrate. The color shows temperature distribution.

For the “hot spot” case, a circular high temperature region having the same temperature profile as above was arranged on the substrate. The substrate temperature as a function of r and θ is given by

$$\begin{aligned} T_w &= T_b + \Delta T \exp(k R^2) \\ R^2 &= (r^2 + r_0^2) - 2rr_0 \cos(\theta - \theta_0) \end{aligned} \quad (17)$$

where the center of the hot spot is located at (r_0, θ_0) .

Thickness Uniformity of Spin Coated Film Influenced by Nonuniform Temperature of Substrates

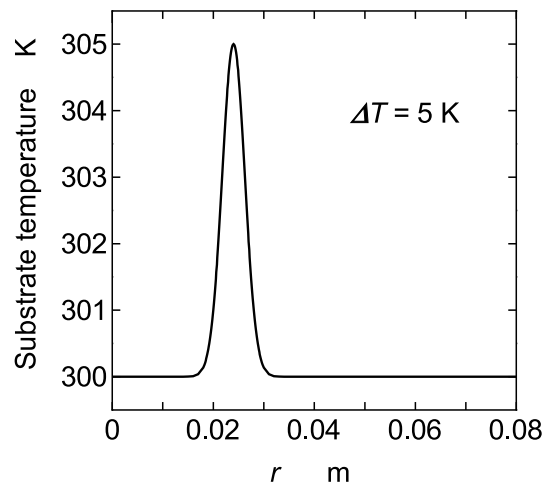
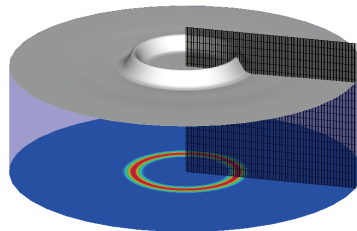
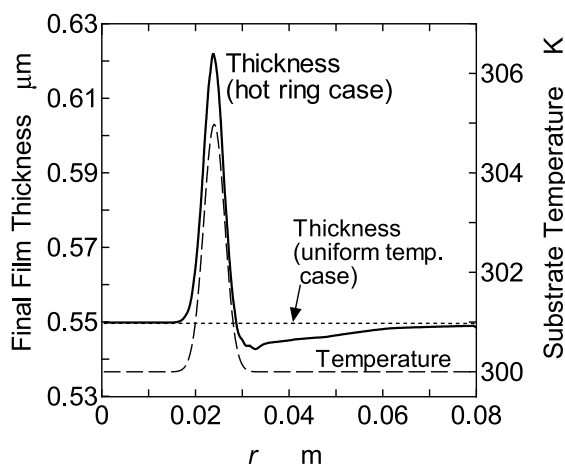


Figure 7. Distribution of substrate temperature of the “hot ring” for the case of $T_b=300$ K and $\Delta T=5$ K.



(a) Profile

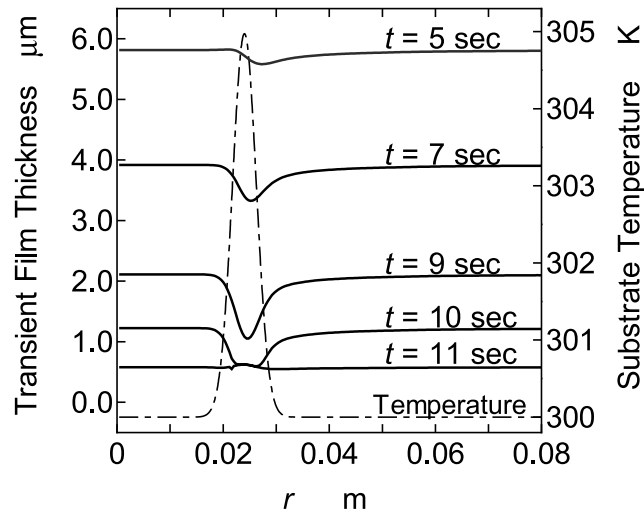


(b) Thickness distribution averaged over θ .

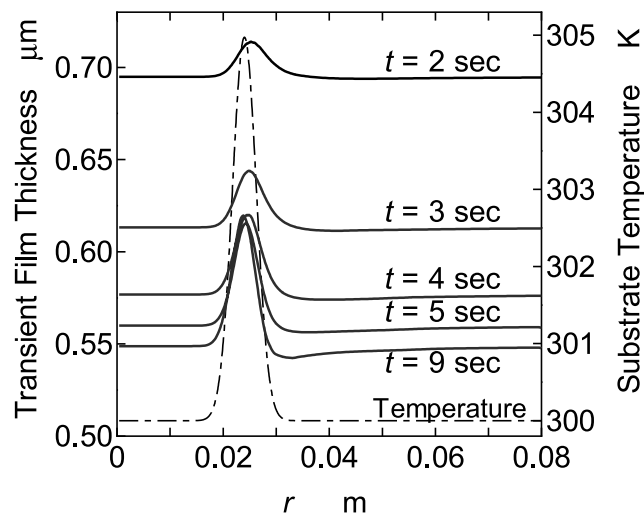
Figure 8. Final thickness of a spin-coated film on a substrate with a “hot ring” for the case with $\Delta T=5$ K, $T_0=T_g=300$ K, $H_0=100$ μm, $C_0=0.06$, and $\omega=100$ rad/s.

Figure 8(a) shows the final profile of the coated film thickness for the “hot ring” case with $\Delta T=5$ K, $T_0=T_g=300$ K, $H_0=100$ μm, $C_0=0.06$, and $\omega=100$ rad/s. The profile is axially symmetrical and no dependency on θ is observed. A bump of a ring shape is clearly observed above the hot ring on the substrate. The final film thickness as a function of r , which is averaged over θ , is shown in Fig. 8(b) with

the distribution of the substrate temperature. The peak of the final film thickness lies exactly on the hot ring. In the region downstream of the bump, the final film thickness is reduced to be smaller than those in the downstream region far from the bump and in the upstream region. The thickness in those regions is almost equal to the final film thickness obtained in the case of uniform substrate temperature.



(a) Transient film thickness, H



(b) Solute portion of the thickness, H_{sl}

Figure 9. Transient film thickness and solute portion of the thickness on a substrate with a “hot ring” for the case with $\Delta=5$ K, $T_0=T_g=300$ K, $H_0=100$ μm , $C_0=0.06$, and $\omega=100$ rad/s.

Figure 9 shows the film thickness in the transient process shown in Fig. 8, where the thickness is averaged over θ and shown as a function of r again. Figures 9(a) and 9(b) show the film thickness of the solution, H , and solute portion of the film thickness, H_{sl} , respectively. As was discussed by eqn (9b), H decreases both by the radial flow of the solution driven by the centrifugal forces and the solvent evaporation, while H_{sl} decreases only by the radial flow of the solution. The transient process observed by Figs. 9(a) and (b) is as follows: The solvent evaporates at the surface of the high temperature region, and H decreases rapidly exhibiting a local minimum in this region. The concentration increase in this high temperature region causes an increase in solution viscosity, and it reduces the radial flow of the solution, which results in a decrease in film thinning rate in this region. Consequently, a bump appears in the final film. The location of the peak is slightly downstream of the center of “hot ring” on the

substrate initially, which is influenced by the radial flow of the solution. As the thickness decreases and approaches the final one, the peak shifts to the center of the “hot ring”.

In the case of a “cold ring”, in which a ring-like region with a lower temperature exists on the substrate, phenomena opposite to the “hot ring” cases occur; the final film thickness above the “cold ring” is smaller than that in the other region, and a ring-like depression appears in the coated film. The final film thickness in the region downstream of the depression is slightly larger than the average thickness. The height of the bump and depression on the “hot/cold ring” of the substrate is shown in Fig. 10 as a function of the peak or bottom temperature given by eqn (16) as $T_b + \Delta T$. Linear relationship is observed between the peak/bottom film thickness and the temperature of the “hot/cold ring” in this temperature range, which is approximately variation of 10% in thickness for the temperature difference of ± 5 K around 300 K.

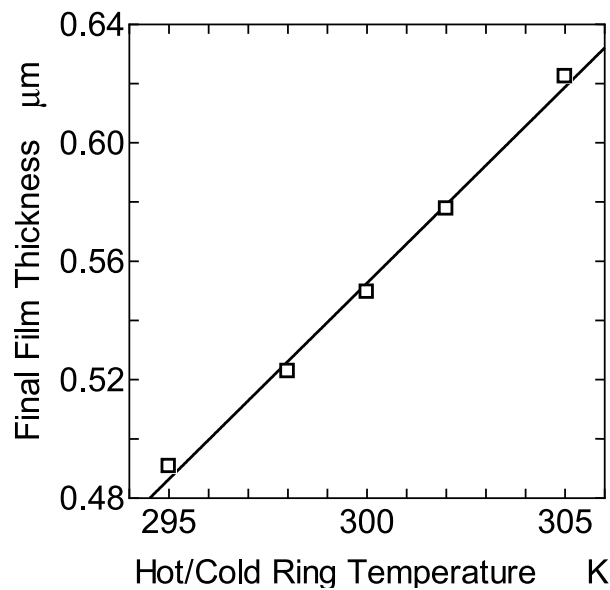
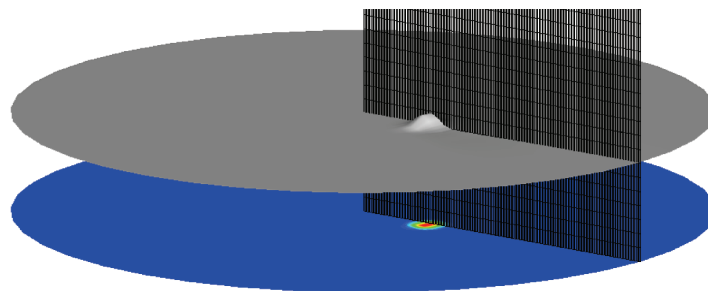


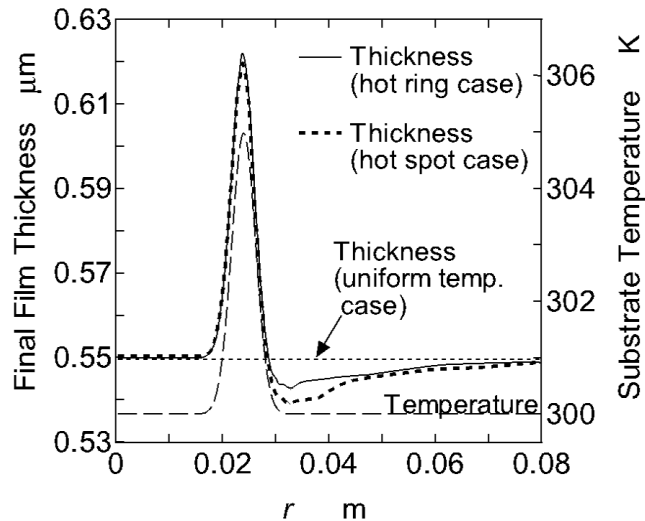
Figure 10. Peak/bottom thickness of the bump/depression on the “hot/cold ring” of the substrate. The straight line fitted to the data (open boxes) is only for clarity.

Figure 11 shows the final film thickness for the “hot spot” case with $\Delta T=5$ K, $T_0=T_g=300$ K, $H_0=100$ μm, $C_0=0.06$, and $\omega=100$ rad/s. In Fig. 11(a), a spot-like bump is observed on the “hot spot” of the substrate. The distribution along r shown in Fig. 11(b) exhibits some characteristics similar to those for the “hot ring” case shown in Fig. 8(b), such as the bump on the hot ring/spot, and the region with decreased thickness downstream of the bump. The height of the peak is almost equal to that of the “hot ring” case, which is clearly demonstrated in Fig. 11(c) for the distribution along θ .

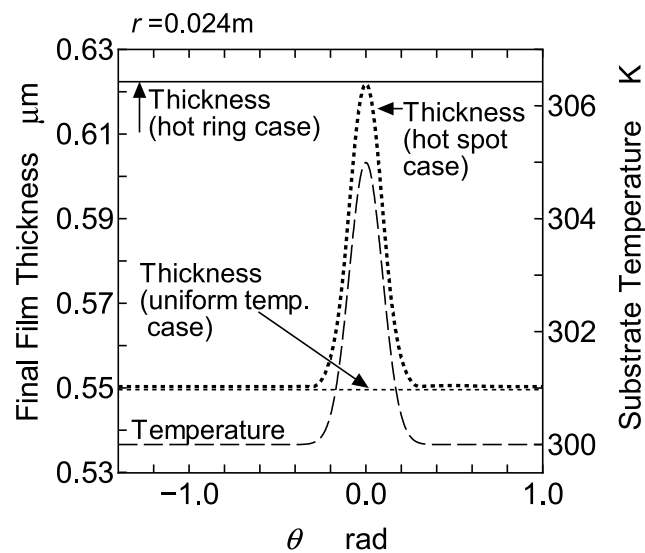


(a) Profile

Figure 11. (continue)



(b) Thickness distribution along r at $\theta = \theta_0$.



(c) Thickness distribution along θ at $r=r_0$.

Figure 11. Final thickness of a spin-coated film on a substrate with a “hot spot” for the case with $\Delta T=5$ K, $T_0=T_g=300$ K, $H_0=100$ μm , $C_0=0.06$, and $\omega=100$ rad/s.

In Fig. 12, the peak/bottom thickness of the bump/depression on the hot/cold spot is compared with those for the hot/cold ring cases shown in Fig. 10 and also with the final film thickness observed for the cases with uniform substrate temperatures shown in Fig. 5. The “hot/cold spot” cases exhibit almost the same response as the “hot/cold ring” cases. These responses are different from those of the uniform temperature cases, i.e., the peak film thickness on the hot ring/spot is larger than the film thickness on the disk of uniform temperature that is equal to the peak temperature of the hot ring/spot.

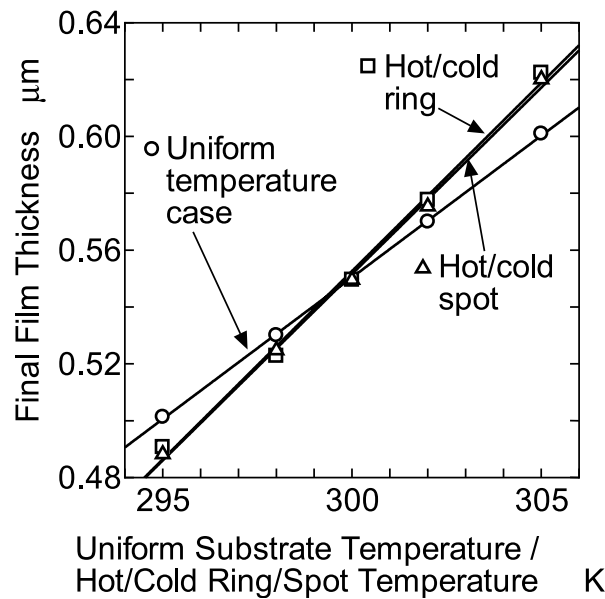


Figure 12. Peak/bottom thickness of the bump/depression on the “hot/cold spot” of the substrate. The results for the “hot/cold ring” cases and the thickness obtained for the uniform temperature cases are compared in the figure. The straight lines fitted to the data are only for clarity.

3.3 Case of film formation on a substrate at rest with nonuniform temperature

A drying process of a solution on the non-spinning substrate is described here for a case with the “hot ring” distribution of substrate temperature. The simulation has been performed for the case with $\Delta T=5$ K, $T_0=T_g=300$ K, $H_0=100$ μm , $C_0=0.06$ and $\omega=0.01$ rad/s. Although the spinning speed is not absolutely zero, this condition provides a well-defined condition for the state of the ambient atmosphere and evaporation of the solvent in a case where radial flow of coating liquid has very little effect in the film thinning process as compared with the solvent evaporation.

The solute portion of the transient and final film thickness, H_{sl} , exhibited the distributions shown in Fig. 13. A peak of a simple shape is formed on the hot ring in the early stage until $t=7000$ s, and after that, the peak drops gradually making the two peaks in the neighbor regions. A clear double ring structure is formed in the final film. The region of the two peaks is wider than the region of temperature peak. Film thickness in the inner and outer regions of the “hot ring” is decreased significantly. This phenomenon results from a complicated balance between mass diffusion of solute and convection of solution driven by hydrostatic pressure; The film thinning rate is increased at the “hot ring” range due to the enhanced evaporation of solvent, which makes radial flow of solution driven by hydrostatic pressure toward the “hot ring” range; the solute is transported toward the position of temperature peak and accumulated there. As the solute concentration is increased in the “hot ring” range, significant increase of viscosity reduces the convection. On the other hand, the accumulation of solute in the “hot ring” range produces steep gradient of solute concentration, which makes mass diffusion of solute from the center of the temperature peak toward inner and outer sides, which reduces the mass of solute at the center of the temperature peak. Consequently, most amount of solute is accumulated off the center of the temperature peak, making two peaks of solute mass in the inner and outer sides.

A factor that may have some influence on the phenomena illustrated here for the cases of the non-spinning substrate is the Marangoni effect which has been neglected in the present study. In this case, the effect works somewhat to reduce the accumulation of solute at the center of the hot range. The exact phenomena in the non-spinning cases, including the above complicated balance of mass transport and the Marangoni effect, should be clarified in the future work.

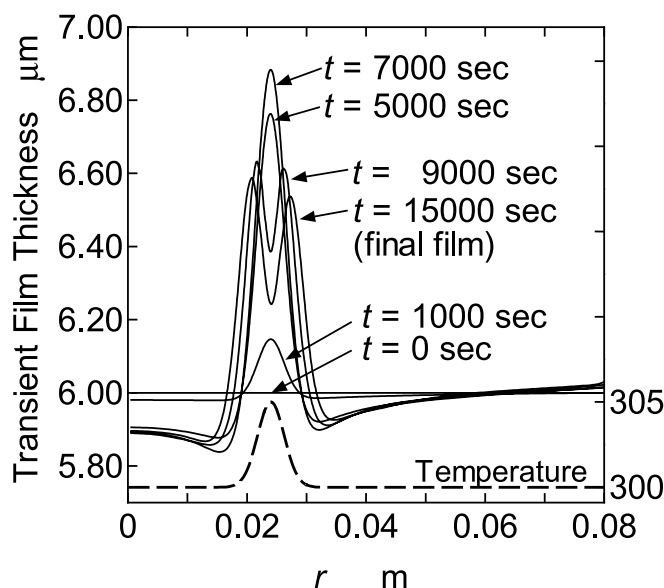


Figure 13. Distribution of the solute portion of the film thickness, H_{sl} , along r for the case of non-spinning substrate with a “hot ring”. $\Delta T=5$ K, $T_0=T_g=300$ K, $H_0=100$ μm , $C_0=0.06$ and $\omega=0.01$ rad/s.

4. CONCLUSION

Heat and mass transfer in the film thinning process during spin coating has been analyzed by 3-D finite difference computational simulations. To examine the influence of nonuniform temperature of the substrate, the cases with a ring-like and spot-like high or low temperature region were analyzed. Obtained results are as follows.

- (1) Final film thickness of the coating film exhibits peak/bottom right on the hot/cold region of the substrate. There is practically no difference in the height of the peak/bottom between the cases of the hot/cold ring and the spot. The film thickness at the peak/bottom is higher than those in the uniform temperature cases where the temperature is equal to the peak/bottom temperature.
- (2) The peak/bottom of the final film thickness is resulted also in the case of non-spinning substrate, where the radial flow of coating liquid driven by the centrifugal forces can be neglected as compared with the solvent evaporation. An interesting film thickness profile that the peak is divided into two peaks was observed, which is caused by a complicated balance between flow of the coating liquid driven by the hydrostatic pressure gradient and mass diffusion.

REFERENCES

- [1] Alekseev, A., Baturin, S., Pavlov, G. and Shiryaev, A., Polymeric film formation in spin coating, *Macromo. Symp.*, 2001, 169, 321–328.
- [2] Schwartz, L. W. and Roy, R. V., Theoretical and numerical results for spin coating of viscous liquids, *Phys. Fluids*, 2004, 16 (3), 569–584.
- [3] Emslie, A. G., Bonner, F. T. and Peck, L. G., Flow of a viscous liquid on a rotating disk, *J. Appl. Phys.*, 1958, 29 (5), 858–862.
- [4] Higgins, B. G., Film flow on a rotating disk, *Phys. Fluids*, 1986, 29 (11), 3522–3529.
- [5] Rehg, T. J. and Higgins, B. G., The effects of inertia and interfacial shear on film flow on a rotating disk, *Phys. Fluids*, 1988, 31 (6), 1360–1371.
- [6] Sukanek, P. C., “Anomalous” speed dependence in polyimide spin coating, *J. Electrochem. Soc.*, 1997, 144 (11), 3959–3963.
- [7] Acrivos, A., Shah, M. J. and Petersen, E. E., On the flow of a non-Newtonian liquid on a rotating disk, *J. Appl. Phys.*, 1960, 31 (6), 963–968.

- [8] Jenekhe, S. A. and Schuldt, S. B., Coating flow of non-Newtonian fluids on a flat rotating disk, *Ind. Eng. Chem. Fundam.*, 1984, 23 (4), 432–436.
- [9] Jenekhe, S. A. and Schuldt, S. B., Flow and film thickness of Bingham plastic liquids on a rotating disk, *Chem. Eng. Commun.*, 1985, 33(1–4), 135–147.
- [10] Sukanek, P. C., Dependence of film thickness on speed in spin coating, *J. Electrochem. Soc.*, 1991, 138 (6), 1712–1719.
- [11] Britten, J. A. and Thomas, I. M., Non-Newtonian flow effects during spin coating large-area optical coatings with colloidal suspensions, *J. Appl. Phys.*, 1992, 71 (2), 972–979.
- [12] Burgess, S. L. and Wilson, S. D. R., Spin-coating of a viscoplastic material, *Phys. Fluids*, 1996, 8 (9), 2291–2297.
- [13] Meyerhofer, D., Characteristics of resist films produced by spinning, *J. Appl. Phys.*, 1978, 49 (7), 3993–3997.
- [14] Jenekhe, S. A., Effects of solvent mass transfer on flow of polymer solutions on a flat rotating disk, *Ind. Eng. Chem. Fundam.*, 1984, 23 (4), 425–432.
- [15] Sukanek, P. C., Spin coating, *J. Imaging Technol.*, 1985, 11, 184–190.
- [16] Bornside, D. E., Macosko, C. W. and Scriven, L. E., Spin coating: one dimensional model, *J. Appl. Phys.*, 1989, 66 (11), 5185–5193.
- [17] Bornside, D. E., Mechanism for the local planarization of microscopically rough surfaces by drying thin films of spin-coated polymer/solvent solutions, *J. Electrochem. Soc.*, 1990, 137 (8), 2589–2595.
- [18] Lawrence, C. J., The mechanism of spin coating of polymer films, *Phys. Fluids*, 1988, 31 (10), 2786–2795.
- [19] Lawrence, C. J., Spin coating with slow evaporation, *Phys. Fluids A*, 1990, 2 (3), 453–456.
- [20] Yonkoski, R. K. and Soane, D. S., Model for spin coating in microelectronic applications, *J. Appl. Phys.*, 1992, 72 (2), 725–740.
- [21] Ohara, T., Matsumoto, Y. and Ohashi, H., The film formation dynamics in spin coating, *Phys. Fluids A*, 1989, 1(12), 1949–1959.
- [22] Flack, W. W., Soong, D. S., Bell, A. T. and Hess, D. W., A mathematical model for spin coating of polymer resists, *J. Appl. Phys.*, 1984, 56 (4), 1199–1206.
- [23] Birnie, D. P. III, Zelinski, B. J. J., Marvel, S. P., Melpolder, S. M. and Roncone, R. L., Film/substrate/vacuum-chuck interactions during spin coating, *Optical Engineering*, 1992, 31 (9), 2012–2020.
- [24] Birnie, D. P. III, Zelinski, B. J. J. and Perry, D. L., Infrared observation of evaporative cooling during spin-coating processes, *Optical Engineering*, 1995, 34 (6), 1782–1788.
- [25] Cobb, E. C. and Saunders, O. A., Heat transfer from a rotating disk, *Proc. R. Soc. Lond. A*, 1956, 236 (1206), 343–351.
- [26] Ohara, T., Ohashi, H. and Matsumoto, Y., Thin film formation on a rotating disk, *Trans. JSME, Ser. B*, 1991, 57 (543), 3807–3814. (in Japanese)